

# We are IntechOpen, the world's leading publisher of Open Access books Built by scientists, for scientists

**4,800**

Open access books available

**122,000**

International authors and editors

**135M**

Downloads

Our authors are among the

**154**

Countries delivered to

**TOP 1%**

most cited scientists

**12.2%**

Contributors from top 500 universities



**WEB OF SCIENCE™**

Selection of our books indexed in the Book Citation Index  
in Web of Science™ Core Collection (BKCI)

Interested in publishing with us?  
Contact [book.department@intechopen.com](mailto:book.department@intechopen.com)

Numbers displayed above are based on latest data collected.

For more information visit [www.intechopen.com](http://www.intechopen.com)



# Monte Carlo Simulations of Grain Growth in Polycrystalline Materials Using Potts Model

Miroslav Morháč<sup>1</sup> and Eva Morháčová<sup>2</sup>

<sup>1</sup>*Institute of Physics, Slovak Academy of Sciences,  
Dubravska cesta 9, 845 11 Bratislava,*

<sup>2</sup>*Faculty of Mechanical Engineering, Slovak University of Technology,  
Namestie Slobody 17, 812 31 Bratislava,  
Slovak Republic*

## 1. Introduction

Sintering of powders is one of the most important processes for the development of polycrystalline materials. The microstructure of a material is of fundamental importance in the processing of ceramics and metals since it affects the physical properties of the final product. Progress in our ability to satisfactorily predict microstructure and its properties has been quite slow owing to complexity of physical processes involved. The complete prediction of microstructural development in polycrystalline solids as a function of time and temperature is a major objective in materials science.

Grain size is a very important characteristic for evaluating properties of the materials, especially when we need to balance different ones [1]. During the sintering of polycrystalline materials the normal grain growth obeys the basic law

$$R = k \cdot t^n, \quad (1)$$

where  $R$  is an average grain size,  $k$  is a constant with Arrhenius temperature dependence,  $t$  is sintering time and  $n$  is a kinetic grain growth exponent. However the grain growth is influenced by many other input parameters.

Recently, computer simulation techniques have been developed, which can successfully incorporate many aspects of the grain interactions and can predict the main features of the microstructure [2-10]. The aim of simulation of polycrystalline grain growth is to approximate to the highest degree to the real structures. Relations between Monte Carlo simulations and real structures have been studied in [11]. A procedure for the simulation and reconstruction of real structures in crystalline solids has been presented in [12]. Experimental and computational studies of grain growth for other various types of materials have been carried out, e.g. in [13-14].

The most realistic correspondence between the evolution of real and simulated structure was achieved by Monte Carlo simulations. Monte Carlo simulation is a stochastic Markov process that generates a sequence of configurations of lattice site states. Trial states are generated from a random distribution and are either accepted or rejected with a probability given by the Boltzmann factor.

The generalized  $Q$ -state Potts spin model is applied to the simulation procedure. The structure development is mapped onto the two-dimensional or three-dimensional discrete simulation lattice. An area element of microstructure is represented by one lattice site and is assigned a random number  $Q_i$  ( $1 < Q_i < Q$ ) called orientation or spin. Grain boundary lies between two adjacent sites with different orientation. The energy of a lattice site is given by the Hamiltonian

$$E = J \sum_{j=1}^n (1 - \delta_{Q_i, Q_j}), \quad (2)$$

where  $J$  is a positive constant,  $Q_i$  is the orientation of the  $i$ -th lattice site,  $Q_j$  is the orientation of the  $j$ -th neighboring lattice site,  $\delta_{Q_i, Q_j}$  is the Kronecker delta. The sum is given over  $n$  vicinal lattice sites.

During the simulation procedure the  $i$ -th lattice site orientation is generated randomly and its energy  $E_1$  is calculated according to (2). Then a new random orientation is given to the  $i$ -th lattice site and energy  $E_2$  after reorientation is again calculated. The reorientation is accepted when  $E_2 < E_1$ . Otherwise the reorientation is accepted with the probability

$$P \approx \exp\{-\Delta E/kT\}, \quad (3)$$

where

$$\Delta E = E_2 - E_1, \quad (4)$$

$k$  is the Boltzmann constant and  $T$  is the temperature. The term  $J/kT$  can be replaced by  $\alpha$  also called temperature factor and for the final probability of the reorientation acceptance one obtains

$$P \approx \exp\{-\alpha d\}. \quad (5)$$

If the 2D lattice consists of  $N \times N$  lattice sites,  $N \times N$  reorientation attempts represent a time unit called Monte Carlo step (MCS). On the other hand for 3D simulation array  $N \times N \times N$  reorientation attempts represent one MCS. In all simulation types described in the contribution the lattice sites can be arranged either in square or hexagonal configuration. The type of the simulation lattice is one of the input parameters before the simulation starts. The influence of this parameter on simulated structure and average grain size was studied in [15].

As mentioned above the initialization of the simulation lattice can be based on random number orientations. However, instead of random number one can employ also experimental orientation. Then the input microstructure can be an experimental one measured either by EBSD (Electron Back Scattered Diffraction) [16] to simulate grain growth or by TEM (Transmission Electron Microscope) to simulate primary recrystallization [17]. Then because the grain orientation is known the grain boundary nature is also known and then its energy can be adjusted (see e.g. [18]). The simulation procedure is universal and the initial simulation lattice can be obtained also from other devices e.g. from REM (Reflection Electron Microscope) [15].

## 2. Normal grain growth simulations

### 2.1 Monophase grain growth

Generally, the simulation algorithm of grain growth is based on the tendency of lattice points to achieve minimum energy. This elementary algorithm of monophase structure development was described in detail, e.g. in [15], [19-20]. An example of grain growth simulation on the 3D square simulation lattice with input parameters  $N = 100$ ,  $Q = 50$ ,  $\alpha = 5$ ,  $t = 1000$  MCS is shown in various display modes in Fig 1.

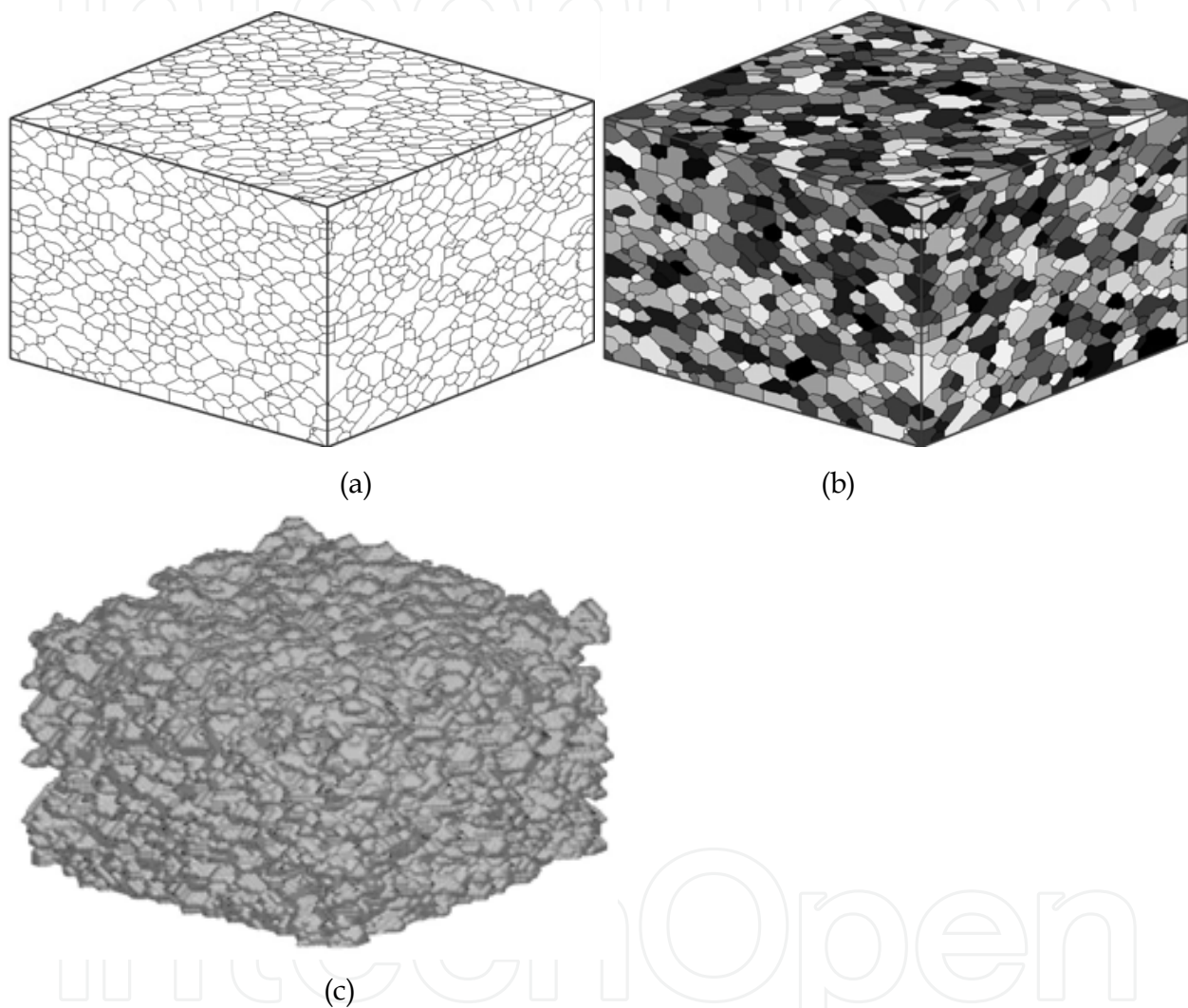


Fig. 1. Grain growth simulated on the 3D square simulation lattice with input parameters  $N = 100$ ,  $Q = 50$ ,  $\alpha = 5$ ,  $t = 1000$  MCS shown in simple display mode a), in shaded grains mode according to  $Q$  b), and shaded surface mode c).

### 2.2 Grain growth with presence of static second phase

The static second phase do not participate in the energy interaction. If during the simulation the lattice point with the orientation  $Q_s$  is randomly chosen this trial is ignored. The simulation continues with another trial. Consequently the positions of the static second phase lattice sites before and after simulation procedure are the same [22-31]. The static second phase lattice points can be arranged either in the form of grain inclusions, whiskers,

fibers. The influence of the input parameters on the simulated microstructure development in Monte Carlo simulations for both monophasic materials and materials containing static second-phase particles has been studied in [32]. An example of 3D grain growth simulation with the static second phase in the form of grains (5%) *a.*, in the form of whiskers (5%) *b.*, and in the form of fibers (10%) *c.* is given in Fig. 2.

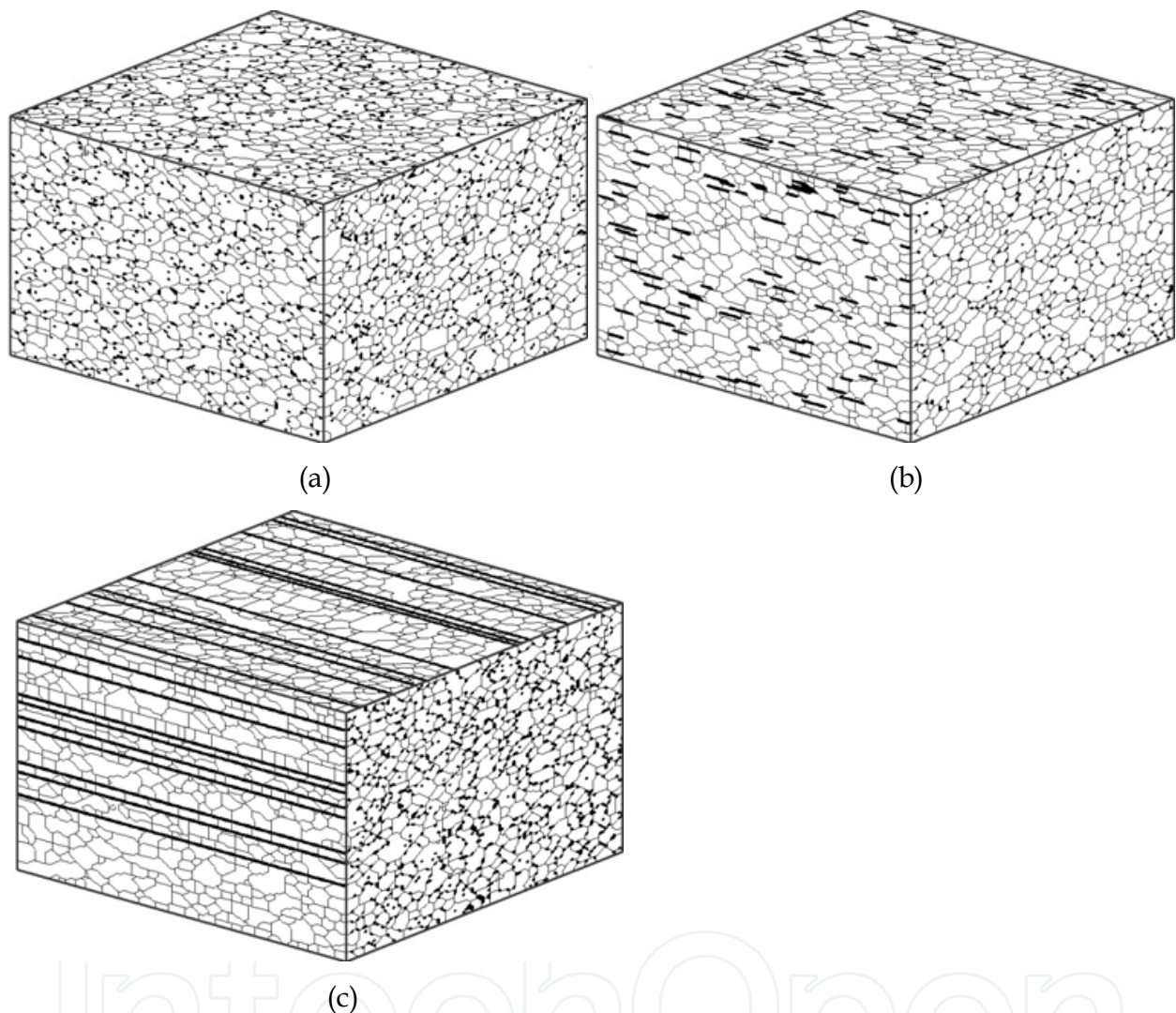


Fig. 2. Grain growth simulated on the 3D simulation lattice with input parameters  $N = 100$ ,  $Q = 50$ ,  $\alpha = 5$ ,  $t = 1000$  MCS with the static second phase in the form of grains (5%) *a.*, in the form of whiskers (5%) *b.*, and in the form of fibers (10%) *c.*

### 2.3 Grain growth in two-phase materials

When simulating grain growth in two-phase materials two types of grains with two different melting temperatures should be taken into account [28-29]. These parameters are represented by two temperature coefficients  $\alpha$  ( $\alpha = J/kT$ ), one for each phase. Then the simulation is carried out analogously to that described, e.g. in [15], [19] with different  $\alpha$  for each phase. An example of biphasic grain growth simulation is illustrated in Fig. 3. Due to both, smaller volume of the second phase grains and smaller  $\alpha$  the grains of the second phase are smaller.

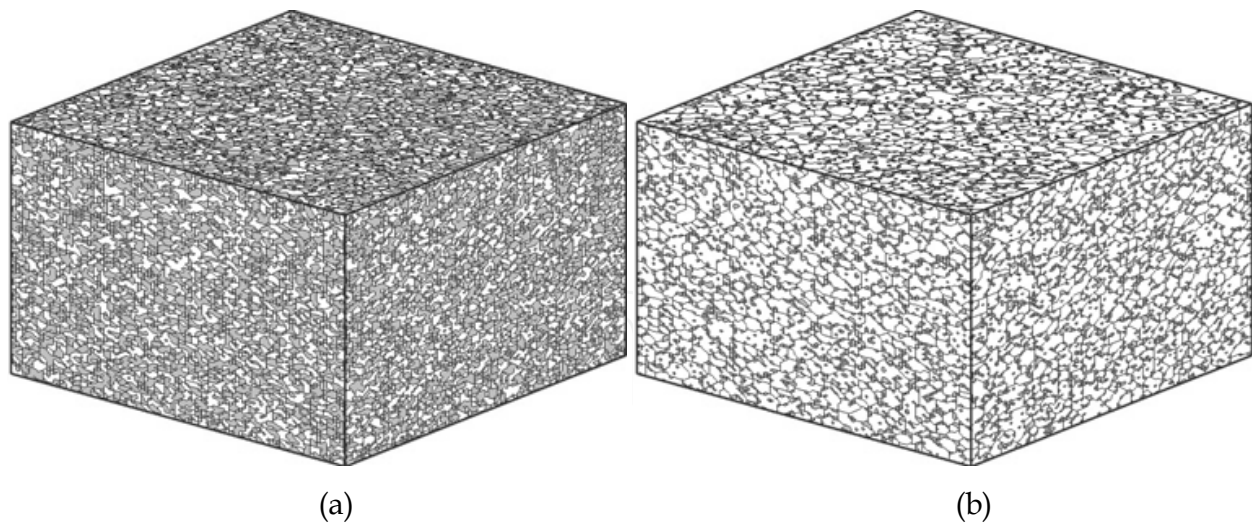


Fig. 3. Biphase grain growth simulated on the 3D simulation lattice with input parameters  $N = 100, Q = 50, t = 1000$  MCS with the second phase volume = 50%,  $\alpha_1 = \alpha_2 = 5$  a), and with the second phase volume = 20%,  $\alpha_1 = 5, \alpha_2 = 1$  b).

#### 2.4 Grain growth with presence of liquid phase

There are many materials, which are prepared by the sintering process under the existence of a liquid phase [30]. In what follows the computer simulation algorithm of the grain growth in the presence of liquid phase is proposed:

- the required percentage of lattice points belonging to the solid phase is initialized randomly with the orientations from the interval  $\langle 1, Q \rangle$ . The rest of lattice points belonging to the liquid phase are initialized with the orientation  $Q_L$ ;
- if the chosen lattice point belongs to the solid phase the reorientation trial follows the algorithm given in [15];
- if the chosen lattice point belongs to the liquid phase with coordinates  $(i_1, j_1)$  so called “mass transfer algorithm” is applied :
  - a. using “random walking algorithm without back step” algorithm [30] we find the first point of the solid phase with coordinates  $(i_2, j_2)$  and orientation  $Q_{Sol}$ ;
  - b. the energy balance at the liquid phase point  $(i_1, j_1)$  is calculated -  $E_{A1}$ ;
  - c. the energy balance at the solid phase point  $(i_2, j_2)$  is calculated -  $E_{A2}$ ;
  - d.  $E_A = E_{A1} + E_{A2}$ ;
  - e. temporarily the solid phase point  $(i_2, j_2)$  is replaced by liquid point and energy balance  $E_{B2}$  is calculated;
  - f. successively for  $k \in \langle 1, Q \rangle$  we calculate the energy balance at the point  $(i_1, j_1)$  and find the smallest  $E_{B1opt}(k)$ ;
  - g.  $E_B = E_{B1opt}(k) + E_{B2}$ ;
  - h. if  $E_B < E_A$  the exchange is accepted. Otherwise the old orientations are left unchanged.

For illustration we introduce the structure development in the presence of liquid phase (shaded lattice points) that was simulated for  $N = 200, Q = 50, t = 100$  MCS,  $\alpha = 5, \gamma_{SL} = 50, \gamma_{SS} = 50$  with 10 % (Fig. 4a) and 40 % (Fig. 4b) of liquid phase  $L$ , respectively. In Fig. 5 we present an example of 3D simulation with liquid phase.

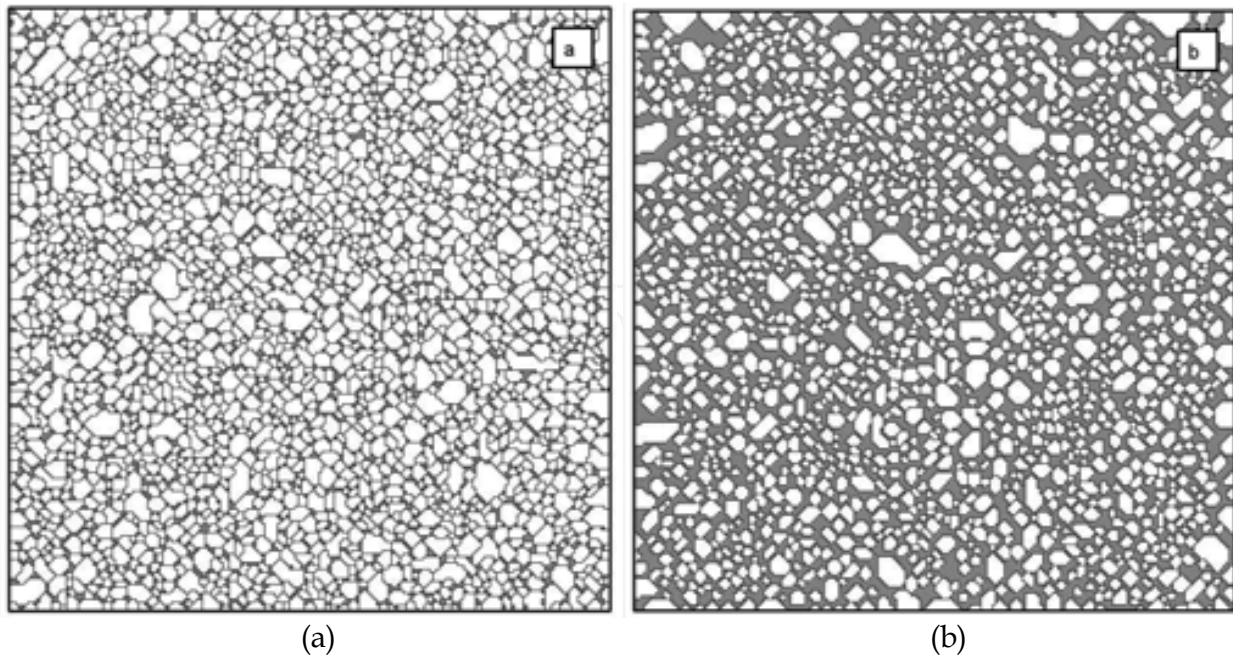


Fig. 4. Grain growth in the presence of liquid phase simulated on the square simulation lattice with input parameters  $N = 200, Q = 50, \alpha = 5, t = 100$  MCS,  $\gamma_{SL} = 50, \gamma_{SS} = 50, L = 10\%$  a) and  $L = 40\%$ , b).

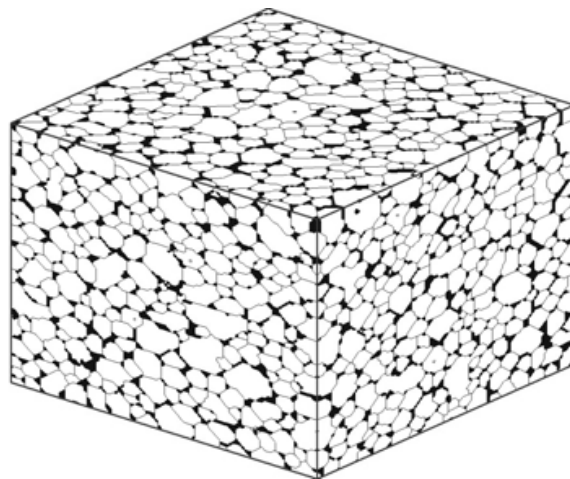


Fig. 5. 3D grain growth simulation in the presence of liquid phase with input parameters  $N = 100, Q = 50, \alpha = 5, t = 200$  MCS,  $L = 20\%, \gamma_{SL} = 50, \gamma_{SS} = 50$ .

### 2.5 Grain growth in the presence of gaseous phase

During the simulation of the structure development of the materials with the presence of dynamical pores, we considered simultaneously the energy balance point of view of solid particles sites as well as the direction of the pores motion aspect [31], [33-35]. In other words along with the simulation of the grain growth through the use of the above given procedures we have to simulate the migration of pores as well. The algorithm of the pore migration involves

- the determination of the direction of the motion
- the calculation of eventual change of the pore position in this direction.

### 2.5.1 Energy balance calculation during pore migration

The kinetics of the pores is realized via the exchange of the orientation of the lattice point  $A$  by the orientation of some of neighboring points, e.g. by the orientation of the point  $B$ . Using (2) we calculate the energy of the pore site  $A - E_{1A}$  and the energy of the site  $B - E_{1B}$ . Then

$$E_1 = E_{1A} + E_{1B}; \quad (6)$$

- we exchange points  $A$  and  $B$ ;
- again using (2) we calculate the energies of both exchanged points -  $E_{2A}, E_{2B}$ . Then

$$E_2 = E_{2A} + E_{2B}; \quad (7)$$

- the difference of the energies before and after the exchange of the points  $A$  and  $B$  is

$$\Delta E = E_2 - E_1; \quad (8)$$

- if  $\Delta E \leq 0$ , the exchange of the sites  $A$  and  $B$  is accepted with the probability equal to 1, otherwise it is accepted with the probability

$$P \approx \exp\{-\beta\Delta E\}, \quad (9)$$

where  $\beta$  is temperature coefficient of the pore motion.

### 2.5.2 Direction of the pore motion

We have studied four models of the pore migrations using different approaches determining the direction of the pore motion. In all the algorithms let us assume that during the simulation we have randomly chosen lattice site  $A$  with  $Q_A = Q_P$ .

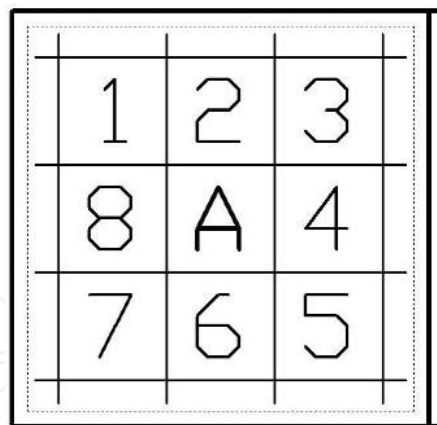


Fig. 6. A part of square simulation lattice with pore lattice site surrounded by lattice points denoted 1 ÷ 8. Double line denotes the nearest edge of the simulation lattice.

#### 2.5.2.1 Stochastic model of the pore motion

In this model, the motion of pores is allowed with equal probability in all directions. The algorithm of the pore motion simulation is as follows:

- in the first step let us denote the 8 lattice points neighboring with the chosen pore site  $A$  by numbers from 1 to 8 according to Fig. 6. Let us assume that the right side of the simulation array (denoted by double line) is the nearest edge (from all 4 edges of the array) to the site  $A$ .



- let us generate the random number (uniform distribution) from the interval  $\langle 1,8 \rangle$  determining the point  $B$  and thus the direction of the eventual pore motion;
- then the energy balance calculation is carried out between these two points according to the algorithm presented in the section 2.5.1. In this model, the motion of pores is allowed with equal probability in all directions. The algorithm of the pore motion simulation is as follows:

### 2.5.2.2 Probability model of the pore motion

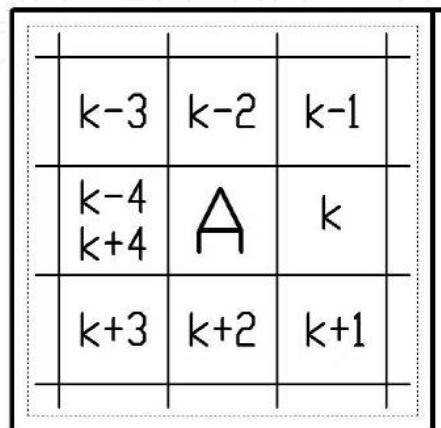


Fig. 7. Distribution of the lattice sites neighboring with the pore site  $A$  and denoted  $k-4 \div k+4$  in the lattice space, where  $k$  is the direction to the nearest simulation lattice edge (double line).

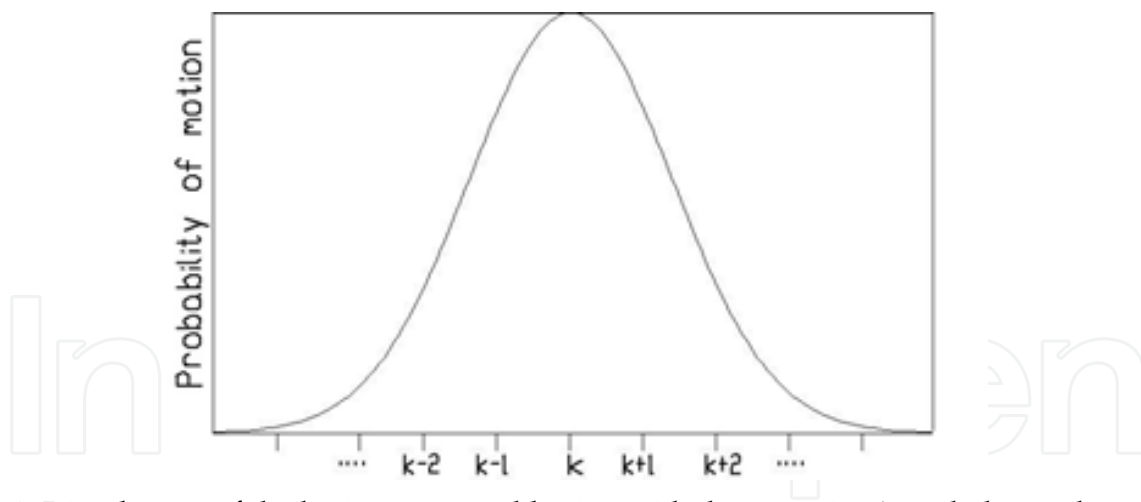


Fig. 8. Distribution of the lattice sites neighboring with the pore site  $A$  and denoted  $k-4 \div k+4$  according to the Gaussian distribution.

In this model, the probability of the pore motion is determined by Gaussian distribution around the direction to the nearest edge of the simulation lattice. The algorithm of the pore motion simulation is as follows:

- we determine the nearest edge of the simulation lattice. The smallest distance to an edge of the lattice is

$$c = \min(X_A, N - X_A, Y_A, N - Y_A), \quad (10)$$

where  $X_A, Y_A$  are the coordinates of the point  $A$  (see Fig. 7). The nearest edge is denoted by double line on the right side of the simulation lattice. We select the direction satisfying (10) and we denote it  $k$ ;

- other lattice points neighboring to the site  $A$  are denoted according to Fig. 7;
- Gaussian random number generator (with  $\sigma$  as input parameter) generates random number from the interval  $\langle k-4, k+4 \rangle$  according to Fig. 8;
- based on this number and using the notation from the Fig. 7 we select neighboring point  $B$ ;
- then the energy balance calculation is carried out between these two points according to the algorithm presented in the section 2.5.1.

### 2.5.2.3 Motion in directions $\langle k-2, k+2 \rangle$ with equal probability - edge model

Using (10) we determine the direction  $k$ . We shall suppose that the pore point  $A$  can interact only with one of the five possible lattice sites denoted in Fig. 9 as  $k-2, k-1, k, k+1, k+2$ . They are symmetrically distributed around the basic direction given by position of the site  $k$ .

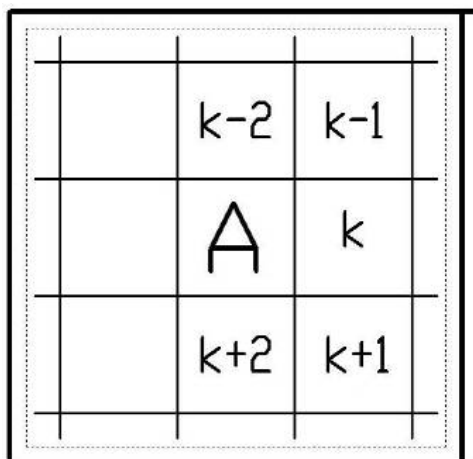


Fig. 9. Lattice point  $A$  surrounded by points denoted  $k-2 \div k+2$ . To define interacting point  $B$  we generate a random number from the interval  $\langle 1, 5 \rangle$  that corresponds to the sites  $k-2, k-1, k, k+1, k+2$ . Then the energy balance calculation is carried out with this point.

### 2.5.3 Results of simulations of pore migration

In Fig. 10a we present final structure after grain growth simulation along with pore migration according to the stochastic model. Due to uniform distribution of the pore motion in all directions, relatively large clusters of pores were enclosed inside of the material. Moreover large amount of small, one point pores (pores of the first generation), remained in the material as well.

In the probability model, it is possible to control the Gaussian distribution of the pores motion. An example of the simulation employing this model for  $\sigma = 2$  is given in Fig. 10b. Only few clusters of pores remained encapsulated. They have regular elliptical shape. One can notice the bent square of solid material in the simulation lattice.

Finally in Fig. 11a we show the resulting structure with pores motion simulation according to the edge model (after 1000 MCS,  $\beta=1000$ ). The majority of pores left the structure and moved to the edges of the simulation lattice. Fewer clusters remained encapsulated inside of the solid material than in the stochastic model. This model like probability model allows to simulate shrinking of pores along with their motion to the edge of the lattice. We can go on with the simulations and change the temperature coefficient of pore migration to  $\beta = 2$ . The structures after 1020 MCS, 1040 MCS and after 5000 MCS are shown in the Figs. 11b, 11c, and 11d respectively. One can see that the encapsulated pores disappeared from the material and the square lattice was straightened.

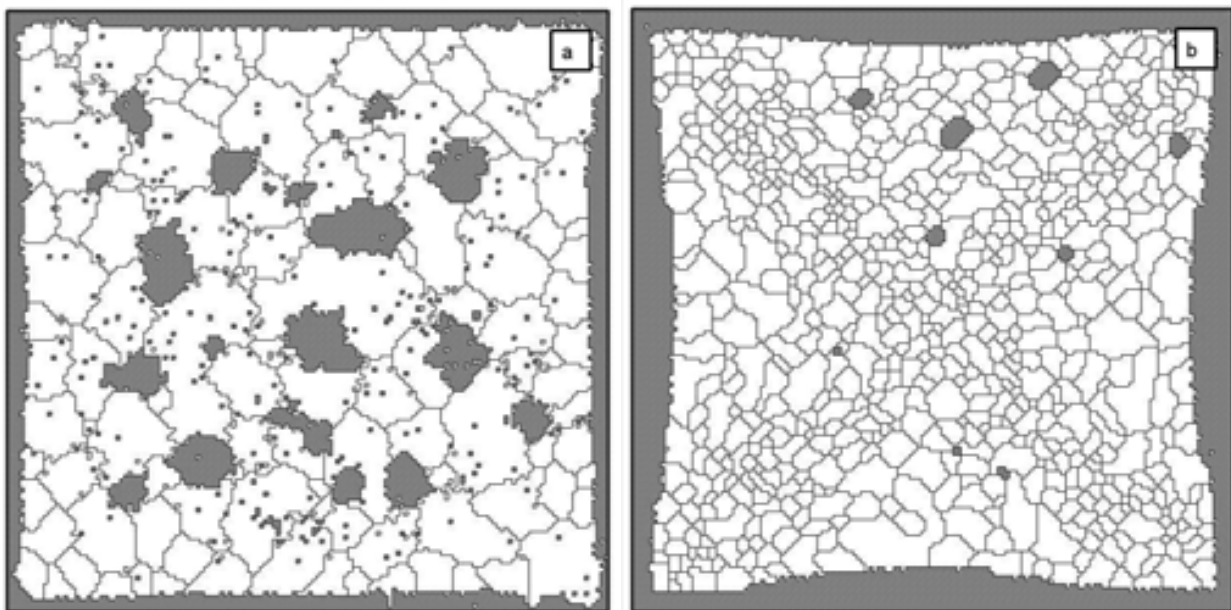


Fig. 10. Grain growth with the mobile pores simulated on the square simulation lattice according to the stochastic model a), the probability model ( $\sigma = 2$ ) b) with input parameters  $N = 150, Q = 40, \alpha = 1000, \beta = 1000, P = 20\%, t = 5000$  MCS.

One can ask why the bent square of the solid material in Fig. 10b is greater than in Fig. 10a and why it completely disappears in Fig. 11d. The difference between both models consists in different probabilities of pores motion. Consequently every model has different speed of the pores motion to the edge of simulation lattice. The aim was to carry out several simulations for both models and to find out which model corresponds to real structures. Actually the sintered ceramic pellets are in fact bent in a way the proposed simulation models indicate.

In Figs. 11 a, b, and c we decreased the temperature coefficient to  $\beta = 2$ . Due to this the pores tend to move to their closest edges of the simulation lattice. In Figs. 11b and c we present intermediate results after 1020 and 1040 MCS, respectively. When we increase dramatically the simulation time to 5000 MCS all pores leave the solid material. However the simulation process of monophasic grain growth in solid material goes on. Due to the finite simulation lattice the pores cannot move in the perpendicular direction towards the edges. They are forced to move along the edges and as a consequence the square lattice is straightened.

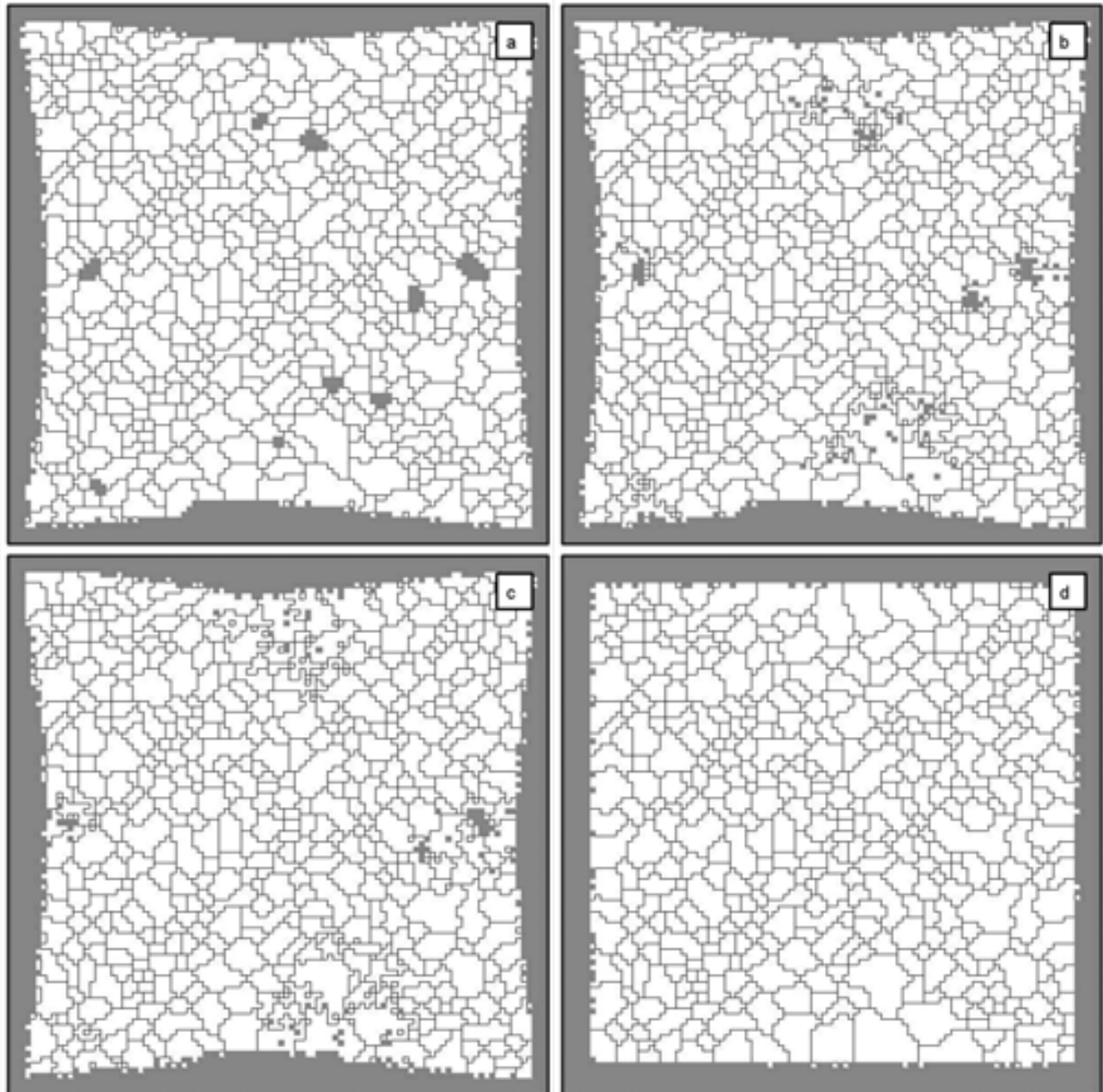


Fig. 11. Grain growth with the mobile pores simulated on the square simulation lattice according to the edge model with input parameters  $N = 100$ ,  $Q = 60$ ,  $\alpha = 1000$ ,  $\beta = 1000$ ,  $P = 20\%$ ,  $t = 1000$  MCS a), then  $\beta = 2$ ,  $t = 1020$  MCS b),  $t = 1040$  MCS c) and  $t = 5000$  MCS.

### 3. Oriented grain growth simulations

#### 3.1 Oriented grain growth in one direction

During the simulation the excess of energy in preferred direction, which determines the grain boundary curvature, can be influenced by changing the value  $J$  in the Hamiltonian (2) in dependence of the neighboring sites [36-38]. It means that neighboring sites contribute with different weights to the Hamiltonian in (2). Hence the Hamiltonian for oriented structures can be written as

$$E = -\sum J(\delta_{Q_i Q_j} - 1), \quad (11)$$

where

$$J = \sum_{j=1}^N J_j. \quad (12)$$

The value  $J_{Pr}$  of the lattice points in the preferred direction equals to the multiple of  $J_{N_i}$  in the non-preferred direction ( $N_i \neq Pr$ ). In practice the preferential grain growth is given by the weights

$$W_i = \frac{J_P}{J_{N_i}}. \quad (13)$$

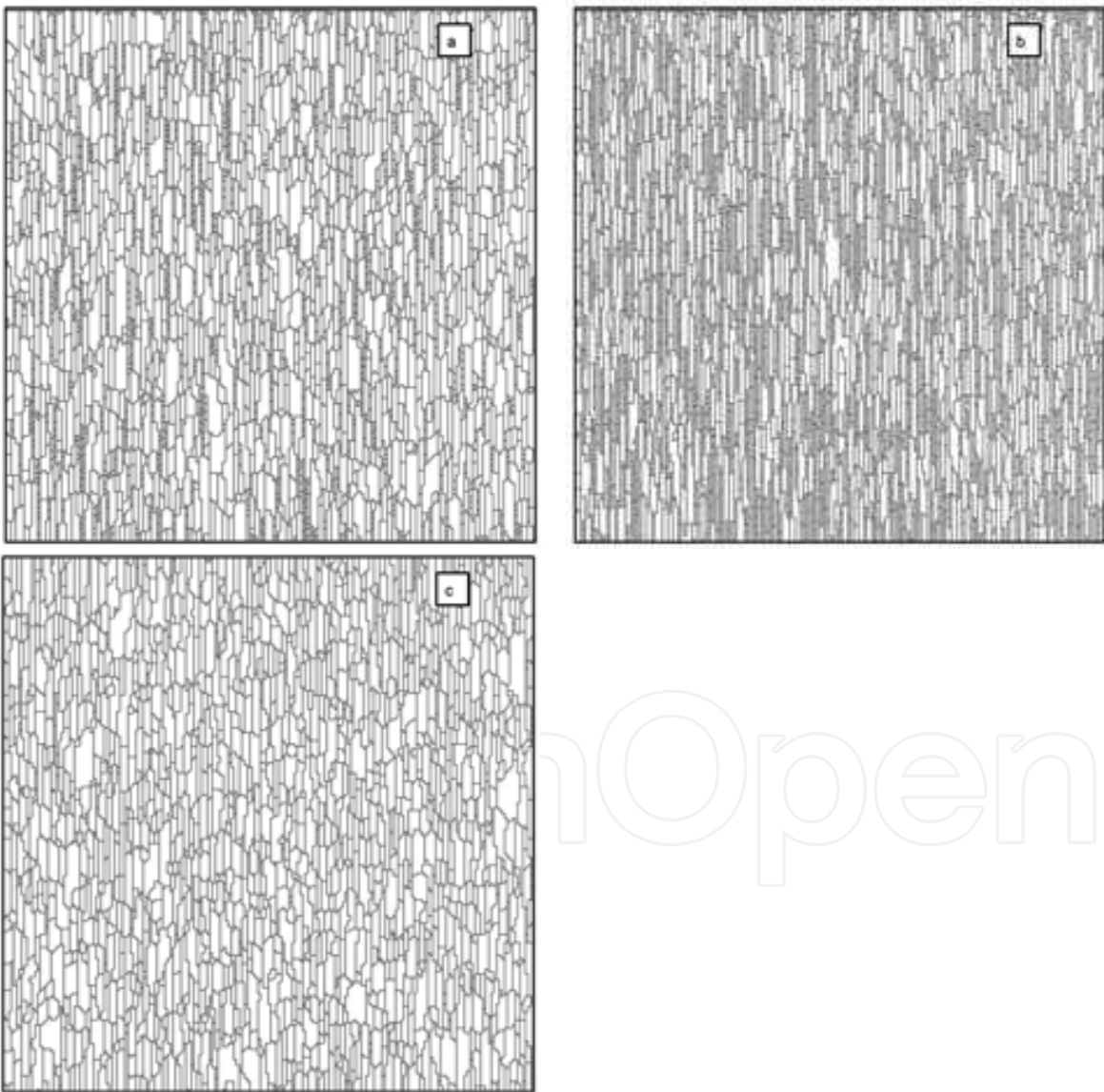


Fig. 12. Oriented grain growth simulated on the square simulation lattice with input parameters  $N = 200$ ,  $Q = 50$ ,  $\alpha = 5$ ,  $t = 1000$  MCS using square model a), cross model b) and elliptical model c). Direction of preferred growth is  $y$ .

In [15] for the square lattice three various algorithms to specify preferred direction were proposed:

1. *two-weights square model* - the weight of grain growth in preferred direction is  $\mathbf{W}_1$ , (horizontal or vertical) the weights of other lattice points neighboring with the point being evaluated are  $\mathbf{W}_2$ .
2. *two-weights cross model* - it allows the evaluated site to interact only with four neighboring sites in horizontal and vertical directions - two points in the preferred direction have the weights  $\mathbf{W}_1$  and two points in the other allowed positions have the weights  $\mathbf{W}_2$ . The neighbors in diagonal directions do not participate in the energy interaction, i.e., their weights are equal to zero.
3. *three-weights elliptical model* - in this model we have proposed three directions - horizontal, vertical and diagonal. The weight  $\mathbf{W}_3$  in diagonal directions is defined by ellipse with semi-axes  $\mathbf{W}_1$  and  $\mathbf{W}_2$  as

$$\mathbf{W}_3 = \mathbf{W}_1 \mathbf{W}_2 \sqrt{2 / (\mathbf{W}_1^2 + \mathbf{W}_2^2)} .$$

To illustrate the influence of the model on the shape of grains in Figs. 12 a - c we present the results of the oriented grain growth with preferred direction  $y$  simulated with the square (a), cross (b) and elliptical (c) models, respectively. In Fig. 13 we present oriented grain growth simulated on 3D simulation lattice using elliptical model with preferred direction  $z$  (a), and preferred directions  $y, z$  (b).

### 3.2 Anisotropic grain growth

#### 3.2.1 Anisotropic grain growth in solid state

While in the oriented grain growth the preferred direction of the growth is the same for all grains in case of anisotropic structures it is related only to a restricted number of grains [39]. The geometrical anisotropic grain growth can be due to crystallographic effects [40]. In the simulation procedure the direction of growth of an anisotropic grain is random. For each anisotropic grain, we assign an arbitrary direction of the growth. For square simulation lattice it is one of the four directions and for triangular simulation lattice it is one of the three directions. Then we proceed according to the following algorithm:

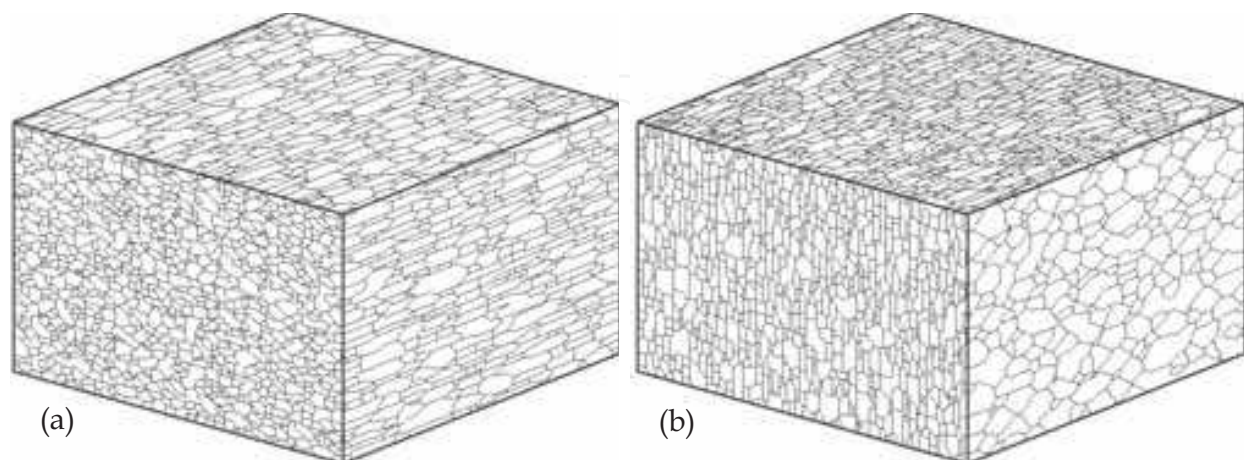


Fig. 13. Oriented grain growth simulated on 3D simulation lattice with input parameters  $N = 100, Q = 50, \alpha = 5, t = 1000$  MCS using elliptical model with weights 1:1:10 a), and 1:10:10 b).

- orientation  $Q$  is divided into two intervals  $\langle 1, Q_E \rangle$  and  $\langle Q_E + 1, Q \rangle$  proportionally to desired percentage  $p_E$  of anisotropic grains, i.e.,  $Q_E = Q - p_E \cdot Q / 100$ ;
- anisotropic lattice points are randomly assigned orientations from the interval  $\langle 1, Q_E \rangle$ ;
- the rest of lattice points, obeying normal grain growth law, are randomly assigned orientations from the interval  $\langle Q_E + 1, Q \rangle$ ;
- for lattice points belonging to normal grains we apply the algorithm described in [15];
- for lattice points belonging to anisotropic grains, we apply the algorithm described in section 3.1 with preferred grain growth direction appertaining to the given orientation of the anisotropic grain.

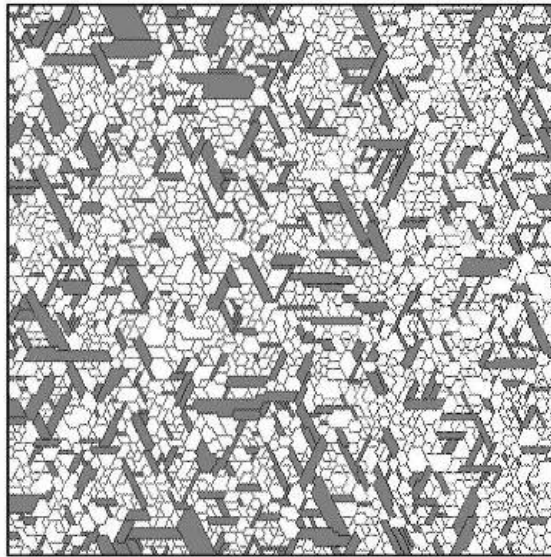


Fig. 14. Anisotropic grain growth according to the elliptical model simulated on the hexagonal simulation lattice with input parameters  $N = 150, Q = 50, \alpha = 5, A = 10\%$ ,  $t = 1000$  MCS and  $W1 : W2 : W3 = 1 : 1 : 20$ .

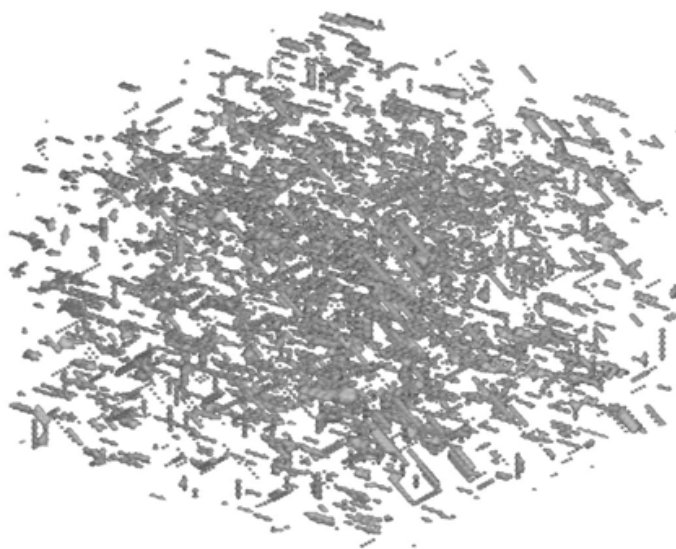


Fig. 15. 3D anisotropic grain growth according to the elliptical model with input parameters  $N = 100, Q = 250, \alpha = 50, A = 5\%$ ,  $t = 1000$  MCS and  $W1 : W2 : W3 = 30 : 1 : 1$ .

In Fig. 14 we show anisotropic grain growth, which was simulated on the hexagonal lattice. The elliptical simulation model with weights ratios  $W1 : W2 : W3 = 1 : 1 : 20$  and with 10% of anisotropic grains (A) (shaded lattice sites) has been chosen. Similar example of 3D anisotropic simulation is given in Fig. 15.

### 3.2.2 Anisotropic grain growth in liquid phase

The above presented simulation algorithm of the grain growth in the presence of liquid phase is dealing with the growth behavior under isotropic energy of solid/liquid interface  $\gamma_{SL}$ . However, in polycrystalline materials there exist material systems (ceramics, cermets, tungsten carbide,  $\alpha$  - alumina, etc), which have the anisotropic behavior of particles during liquid phase sintering [30], [41-42]. If the neighbor of a solid particle is the simulation site corresponding to the liquid phase the energy balance is calculated according to the following algorithm:

- for energies of the interface between solid particles and a liquid phase  $\gamma_{SL}$  ( $\gamma_{SL} \in \langle 0,1 \rangle$ ) and between solid and solid particles  $\gamma_{SS}$  ( $\gamma_{SS} \in \langle 0,1 \rangle$ ) it holds

$$\gamma_{SS} > \gamma_{SL};$$

- let us denote

$$a = \gamma_{SL}$$

$$b = (\gamma_{SS} - \gamma_{SL})/3;$$

- the direction of the interaction for square lattice

$$direction = Q \bmod 4$$

and for hexagonal lattice

$$direction = Q \bmod 3,$$

where Q is the orientation of the solid particle lattice site. The  $direction_i$  is chosen according to the position of the neighbor and the chart shown in Fig. 16a, e.g. for the point B in Fig. 16b the  $direction_i = 2$ .

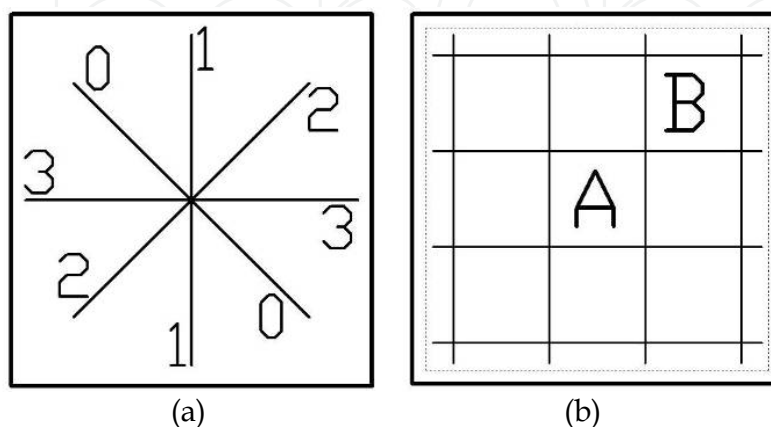


Fig. 16. The chart of possible positions of the neighbors a) and corresponding point B if the position was chosen 2 b).



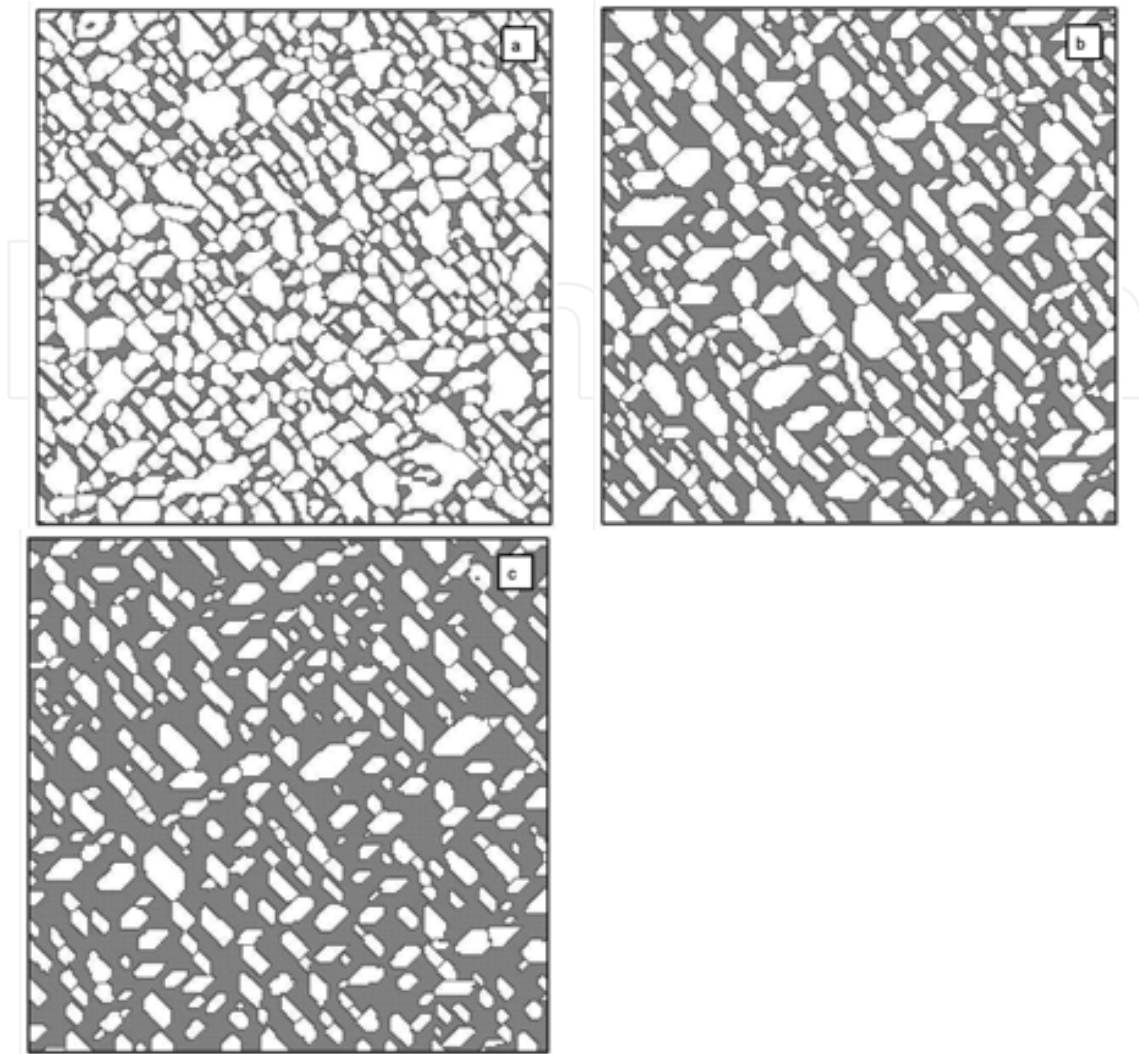


Fig. 17. Anisotropic grain growth in the presence of liquid phase simulated on the hexagonal simulation lattice with input parameters  $N = 200, Q = 50, \alpha = 5, A = 100\%, t = 1000$  MCS,  $\gamma_{SL} = 10, \gamma_{SS} = 90$  and  $L = 20\%$  a),  $40\%$  b),  $60\%$  c).

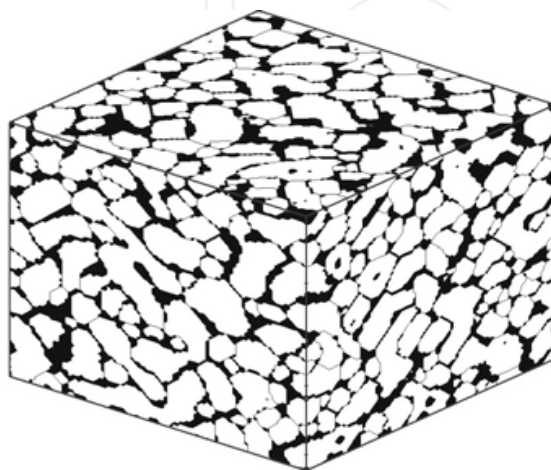


Fig. 18. 3D grain growth simulation in the presence of liquid phase with input parameters  $N = 100, Q = 50, \alpha = 5, t = 200$  MCS,  $L = 20\%, \gamma_{SL} = 10, \gamma_{SS} = 90$ .

- then the increase of the energy in energy balance calculation around the solid particle for the  $direction_i$  is

$$a + b * (3 - |direction - direction_i|)$$

The simulated structures with anisotropic grain growth in liquid phase are shown in Fig. 17 with concentrations of liquid  $L = 20\%$  a),  $40\%$  b) and  $60\%$  c, respectively. In Fig. 18 we give an example of 3D anisotropic grain growth simulation in the presence of liquid phase with input parameters  $N = 100, Q = 50, \alpha = 5, t = 200$  MCS,  $L = 20\%, \gamma_{SL} = 10, \gamma_{SS} = 90$ .

#### 4. Conclusion

In the contribution, we have given an account of various simulation algorithms of the grain growth in polycrystalline materials. We have presented sophisticated algorithms of pore migration, simulation of grain growth in presence of liquid, in oriented and anisotropic structures. All the algorithms have been extended to the three-dimensional simulation arrays. Different input parameters can influence the average grain size, which is very important parameter because it is closely connected with many properties of simulated structures. It can be obtained by scanning the whole simulation lattice using intercept length method. Histograms of the studied parameters are automatically recorded during the simulation.

The average grain size decreases with increasing number of orientations  $Q$ . It is a factor that refers to the particle size distribution in real powders. The simulation carried out for small value of  $Q$  results in small number of irregular grains. On the contrary, the high value of  $Q$  gives small and regular grains similar to the monodisperse particle distribution. Another important parameter that influences the average grain size is simulation time. The study of dependence of this parameter on time has shown that to obtain stable simulation structure the simulation time 1000 MCS is sufficiently long. In [32] the detailed study of the dependence of the size of simulation lattice, type of simulation lattice (square or hexagonal), number of orientations  $Q$ , temperature coefficient  $\alpha$ , etc. on the average grain size was carried out and the results discussed.

The simulation algorithms presented above were implemented in the software package WinSimul, which was developed at the Institute of Physics, Slovak Academy of Sciences. It allows to simulate the structure development, to evaluate the simulated structures, to display lattice during simulation or to record display frames in time in the form of AVI files. It also can display simulation results in the form of average grain size, average area and neighbors (topological) histograms or time dependences of these parameters. It is possible to display several simulations or simulation results simultaneously for various input parameters.

A modular structure of the program WinSimul provides a great flexibility of simulation configurations. Presented work shows only some possible combinations from many others, which may occur in practice.

#### 5. References

- [1] Ling, S. and Anderson, M. P.: Jom, 44, 1992, p.30.
- [2] Matsubara, H. – Furukawa, K. – Brook, R. J.: In: Proceedings 4<sup>th</sup> Euro-Ceramics Society Conference, Eds.: B.S.Tranchina, A.Bellosi, Gruppo Editoriale Faenza Editrice, Riccione, Italy, 1995, p. 597.

- [3] Kurtz, S. K. – Carpay, F. M. A.: *J. Appl. Phys.* 51, 1980, p.5745.
- [4] Anderson, M. P. – Grest, G. S. – Srolovitz, D. J.: *Phil. Mag. B* 59, 1989, p. 293.
- [5] Rollet, A. D. – Luton, M. J. – Srolovitz, D. J.: *Acta Metall. Mater.* 40, 1992, p.43.
- [6] Petzak, P. – Luton, M. J.: *Springer Proceedings in Physics*, 76, 1993, p. 46.
- [7] Hassold, G. N. – Holm, E. A.: *Computers in Physics*, 7, 1993, p. 97.
- [8] Morháčová, E.: *Cryst. Res. Technol.*, 29, 1994, K99.
- [9] Blikstein, P. – Tschiptschin, A. P.: *Mat. Res.* 2, 1999, p. 133.
- [10] Miller, R. S. – Cao, G. – Grujicic, M.: *J. Mater. Synth. Process*, 9, 2001, p. 329.
- [11] Morháčová, E.: *Cryst. Res. Technol.*, 30, 1995, K9.
- [12] Rahman, S. H.: *Acta Cryst.* 49, 1993, p. 56.
- [13] Blikstein, P. – Tschiptschin, A.P.: *Mat. Res.* 2, 1999, p. 133.
- [14] Tajika, M. – Nomura, H. – Matsubara, H. – Rafaniello, W.: *J. Ceram. Soc. Japan* 109, 2001, p. 288.
- [15] Morháč, M. – Morháčová, E.: *Cryst. Res. Technol.*, 35, 2000, p. 117.
- [16] Baudin, T. – Paillard, P. – Penelle, R.: *Script. Mater.* 36, 1997, p. 789.
- [17] Baudin, T. – Julliard, F. – Paillard, P. – Penelle, R.: *Script. Mater.* 43, 2000, p. 63.
- [18] Caleyó, F. – Baudin, T. – Paillard, P. – Penelle, R.: *Script. Mater.* 46, 2002, p. 829.
- [19] Tikare, V. – Cawley, J. D.: *J. Am. Ceram. Soc.* 81, 1998, p. 485.
- [20] Raabe, D. – Roters, F. – Barlat, F. – Chen, L. Q.: *Continuum Scale Simulation of Engineering Materials: Fundamentals – Microstructures – Process Applications*, Weinheim, Wiley-VCH Verlag GmbH & Co. KGaA, 2004
- [21] Yabushita, S. – Hatta, N. – Kikuchi, S. – Kokado, J.: *Script. Metall. Mater.* 19, 1985, p. 853.
- [22] Doherty, R. D. – Li, K. – Kashyup, K. – Rollet, A. D. – Anderson, M. P.: In: *Proc. of Tenth Risø International Symposium on Metallurgy and Material Science : Materials Architecture*, Eds.: J.B. Bilde-Sorensen et al., Risø National Laboratory, Roskilde, Denmark, 1989, p. 31.
- [23] Anderson, M. P. – Grest, G. S. – Doherty, R. D. – Li, K. – Srolovitz, D. J.: *Script. Metall. Mater.* 23, 1989, p. 753.
- [24] Hassold, G. N. – Holm, E. A. – Srolovitz, D. J.: *Script. Metall. Mater.* 24, 1990, p. 101.
- [25] Hazzeldine, P. M. – Oldershaw, R. D. J.: *Phil. Mag. A* 61, 1990, p. 579.
- [26] Olguín, A. et al.: *Phil. Mag. B* 81, 2001, p. 731.
- [27] Yoshikiro, S. – Yoshiyuki, S. – Hideiro, O.: *Script. Mater.* 55, 2006, p. 407.
- [28] Cahn, J.W. – Holm, E. A. – Srolovitz, D. J.: *Mat. Sci. Forum* 94-96, 1992, p. 141.
- [29] Zheng, Y. G. et al.: *Appl. Phys. Lett.* 88, 2006, 144103.
- [30] Matsubara, H. – Furukawa, K. – Brook, R. J.: In: *Proceedings 4<sup>th</sup> Euro-Ceramics Society Conference*, Eds.: B.S.Tranchina, A.Bellosi, Gruppo Editoriale Faenza Editrice, Riccione, Italy, 1995, p. 529.
- [31] Hassold, G. N. – Srolovitz, D. J.: *Scripta Metall. et Mater.* 32, 1995, p. 1541.
- [32] Morháčová, E. – Morháč, M.: *Kovove Mater.* 45, 2007, p. 105.
- [33] Chen, I. W. – Hassold, G. N. – Srolovitz, D. J.: *J. Amer. Ceram. Soc.* 73, 1990, p. 2865.
- [34] Morháčová, E.: *Cryst. Res. Technol.*, 30, 1995, K4.
- [35] Tikare, V. – Miodownik, M. A. – Holm, E. A.: *J. Am. Ceram. Soc.* 84, 2001, p. 1379.
- [36] Vaz, M. F. – Soares, A. – Fortes, M. A.: *Scripta Metall. et Mater.* 24, 1990, p. 2453.
- [37] Tavernier, P. – Szpunar, J. A. : *Acta Metall. et Mater.* 39, 1991, p. 549.
- [38] Tavernier, P. – Szpunar, J. A. : *Acta Metall. et Mater.* 39, 1991, p. 557.
- [39] Kunaver, U. – Kolar, D.: *Mat. Sci. Forum* 94-96, 1992, p. 785.
- [40] Baudin, T. – Paillard, P. – Penelle, R.: *Script. Mater.* 40, 1999, p. 1111.
- [41] German, R. M.: *Liquid phase sintering*, New York, Plenum Press, 1985.
- [42] Sebaugh, M.M. – Kerscht, I. H. – Messing, G. L.: *J. Am. Ceram. Soc.*, 80, 1997, p. 1181.



## **Applications of Monte Carlo Method in Science and Engineering**

Edited by Prof. Shaul Mordechai

ISBN 978-953-307-691-1

Hard cover, 950 pages

**Publisher** InTech

**Published online** 28, February, 2011

**Published in print edition** February, 2011

In this book, Applications of Monte Carlo Method in Science and Engineering, we further expose the broad range of applications of Monte Carlo simulation in the fields of Quantum Physics, Statistical Physics, Reliability, Medical Physics, Polycrystalline Materials, Ising Model, Chemistry, Agriculture, Food Processing, X-ray Imaging, Electron Dynamics in Doped Semiconductors, Metallurgy, Remote Sensing and much more diverse topics. The book chapters included in this volume clearly reflect the current scientific importance of Monte Carlo techniques in various fields of research.

### **How to reference**

In order to correctly reference this scholarly work, feel free to copy and paste the following:

Miroslav Morháč and Eva Morháčová (2011). Monte Carlo Simulations of Grain Growth in Polycrystalline Materials Using Potts Model, Applications of Monte Carlo Method in Science and Engineering, Prof. Shaul Mordechai (Ed.), ISBN: 978-953-307-691-1, InTech, Available from:

<http://www.intechopen.com/books/applications-of-monte-carlo-method-in-science-and-engineering/monte-carlo-simulations-of-grain-growth-in-polycrystalline-materials-using-potts-model>

# **INTECH**

open science | open minds

### **InTech Europe**

University Campus STeP Ri  
Slavka Krautzeka 83/A  
51000 Rijeka, Croatia  
Phone: +385 (51) 770 447  
Fax: +385 (51) 686 166  
[www.intechopen.com](http://www.intechopen.com)

### **InTech China**

Unit 405, Office Block, Hotel Equatorial Shanghai  
No.65, Yan An Road (West), Shanghai, 200040, China  
中国上海市延安西路65号上海国际贵都大饭店办公楼405单元  
Phone: +86-21-62489820  
Fax: +86-21-62489821

© 2011 The Author(s). Licensee IntechOpen. This chapter is distributed under the terms of the [Creative Commons Attribution-NonCommercial-ShareAlike-3.0 License](#), which permits use, distribution and reproduction for non-commercial purposes, provided the original is properly cited and derivative works building on this content are distributed under the same license.

IntechOpen

IntechOpen